JOM, Vol. 71, No. 3, 2019
https://doi.org/10.1007/s11837-018-3216-2

SOLID FREEFORM FABRICATION

Effect of Initial Surface Features on Laser Polishing of Co-Cr-Mo Alloy Made by Powder-Bed Fusion

B. RICHTER,[1] N. BLANKE,[2] C. WERNER,[2] F. VOLLERTSEN,[2,3] and F.E. PFEFFERKORN[1,4]

1.—Department of Mechanical Engineering, University of Wisconsin - Madison, Madison WI 53706, USA. 2.—Bremer Institut für angewandte Strahltechnik GmbH, 28359 Bremen, Germany. 3.—University of Bremen, 28359 Bremen, Germany. 4.—e-mail: frank.pfefferkorn@wisc.edu

One of the challenges regarding widespread use of parts created by the powder-bed fusion process is their high surface roughness, which necessitates some type of postbuild finishing process. Laser polishing (i.e., remelting), which uses surface-tension-driven flow to reduce the roughness of irradiated metallic surfaces, is one such potential finishing process. This work examines the effect that surface features on the as-built part have on the performance of continuous-wave laser remelting of Co-Cr-Mo alloy (Celsit 21-P, Stellite 21 equivalent) samples produced by powder-bed fusion manufacturing. This is accomplished by comparison of three-dimensional surface measurements before and after laser remelting using focus-variation microscopy. Engineering models used to simulate the surface profile as a result of laser remelting are also presented. The results from this work provide insight into the fundamental physics occurring during laser remelting on parts made by powder-bed fusion and will aid parameter selection for surface consolidation and smoothing.

INTRODUCTION

Additive manufacturing has seen rapid growth over the past few years due to the innovative and complex parts that can be created using such layer-by-layer fabrication techniques.[1] However, numerous challenges to final part production with additive manufacturing techniques exist, including the high surface roughness found on parts created using powder-bed fusion additive manufacturing methods. Surface roughness not only results in undesirable esthetic quality but reduces part performance such as fatigue life.[2] This has made understanding of the created surface and the best techniques for its measurement a critical area of study in the field of additive manufacturing.[3–5] It has also driven study on suitable finishing techniques such as electrical discharge machining,[2] sandblasting,[6] electrochemical polishing,[7] and chemical etching.[7,8] Laser polishing by remelting, where a laser locally melts a region of the surface and surface-tension-driven flow smooths the surface,[9] is another potential finishing method that is advantageous due to its contactless, selective, and highly controllable nature.

It has been demonstrated that laser polishing can improve the surface roughness of steel, aluminum, titanium, and cobalt-chromium parts made using powder-bed fusion processes.[10–18] The typical approach used in these works when studying the effect of laser polishing on the surface roughness was to measure multiple regions before and after laser polishing, so the regions measured before and after laser polishing were typically not the same. Thus, the effect of laser polishing was studied by statistical inference from multiple measurements of the surface before and after. However, a challenge when measuring different regions before and after polishing is that the initial surface roughness may vary significantly across the part or different laser-polished areas; For example, in this work, different regions before laser polishing showed average roughness in the range from 13.77 μm to 23.09 μm.

(Published online November 20, 2018)

Numerous models have been created to model the surface after laser polishing. One approach views the surface as idealized close-packed hemispheres or another geometric shape and models the energy needed to melt or ablate the surface.[19–21] Another approach uses experimental results and generalized linear models to predict the surface following remelting.[11] A final approach uses spatial frequency analysis of the surface to analyze how individual spatial frequencies get dampened during remelting. This approach utilizes a critical frequency, derived from capillary wave fluid dynamics, which predicts the frequencies that get dampened over a specified melt duration.[22] This concept has been used to create a model for laser polishing of surface features using a low-pass Gaussian filter.[23] This work was later expanded to predict features created from Marangoni, or thermocapillary, flow during pulsed laser polishing based on analytical and experimental relationships between the melt duration and induced features.[24–26]

This critical frequency method has only been applied to pulsed laser polishing due to the difficulty in estimating the melt duration for continuous-wave laser polishing because of accumulated heat that builds up when laser polishing areas. This work applies the spatial frequency method for continuous-wave laser polishing of individual lines. This negates the thermal buildup effect and allows for melt duration estimation. A method is presented for melt duration estimation based on geometric relationships between experimental and simulated melt pools. This work also measures the same region before and after laser polishing based on reference lines on the surface. This was done to better study how individual particles consolidate into the surface during the remelting process and to consider the effect of localized regions of high or low roughness.

MATERIALS AND METHODS

Materials

The additive-manufactured samples used in this study were made from Co-Cr-Mo alloy (Celsit 21-P, Stellite 21 equivalent) using a powder-bed fusion process (SLM 250, SLM Solutions). The composition of the alloy, and its properties used for the melt time and critical frequency calculations, are presented in Table I. The thermophysical properties listed were used in both the capillary smoothing surface prediction model and in finding solutions to the heat equation for estimating the melt duration. The nominal powder diameter was 20–53 μm, and each layer during the build process was 100 μm thick. The build process used a 60-μm-diameter laser spot with power of 110 W and scan speed of 158 mm/s. The parts were rectangular with final built dimensions of 20.5 mm × 9.4 mm × 3.4 mm. An example of a part used in this experiment is shown in Fig. 1. The side of the part (surface normal to the build direction) was the region of interest for laser polishing in this study, due to its higher initial surface roughness than the top surface.

The absorption of the sample to 1070 nm light for the simulation model was approximated as 36.4% (based on a compositional average of the absorption of cobalt, nickel, chromium, and molybdenum at the 1070 nm wavelength[27]). Due to the high roughness of the surface, it would be expected that the actual absorption would be higher due to reabsorption of the diffusive reflectance of the laser onto partially adhered particles on the surface. The solidus temperature, 1568 K,[28] was defined as the melting temperature of the material for the purpose of melt time estimation.

Laser Polishing Experiments and Analysis

Laser polishing experiments were performed on the sides of the additive-manufactured samples orthogonal to the build direction using a 200-W, 1070-nm fiber laser (SPI Lasers, SP-200C-W-S6-A-B) with a Gaussian-shaped beam operated in continuous-wave mode. The experiments consisted of nine individual 1.5-mm-long lines polished using various beam diameters, heat fluxes, and velocities. An example of the surface before and after laser polishing is shown in Fig. 2. A crack can be seen on the right side of the image, believed to have occurred during solidification.

The beam diameter was controlled by defocusing the beam away from the focal plane. The relationship between the beam flux and power is given in Eq. 1. Results are also presented using the energy density, calculated using Eq. 2. The energy density is a convenient parameter that captures the three controllable laser parameters and has been shown to influence the final roughness after laser polishing.[11,32]

$$\text{Beam Flux} = \frac{4P}{\pi D^2} \quad (1)$$

Table I. Celsit 21-P composition (analysis provided by manufacturer) and thermophysical properties (at room temperature unless stated)

Cr (%)	Mo (%)	Ni (%)	Others (< 3.348%)	Co (%)	Specific heat (J/kg K)[29]	Thermal conductivity (W/m K)[28]	Density (kg/m^3)[30]	Viscosity (Pa s) (Co, 1800 K)[31]
26.6	5.28	2.74	B, C, Fe, P, Si	Bal.	502	14.5	8330	4.54×10^{-3}

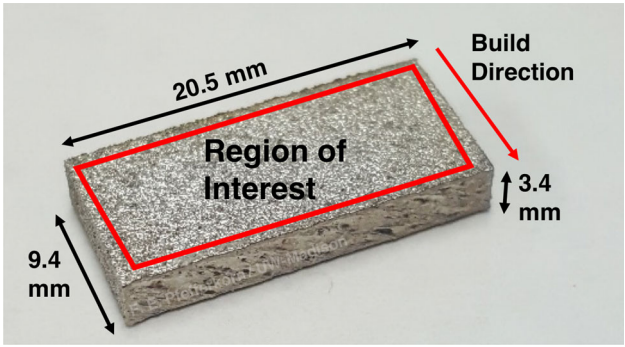

Fig. 1. Part under study and region of interest for laser polishing.

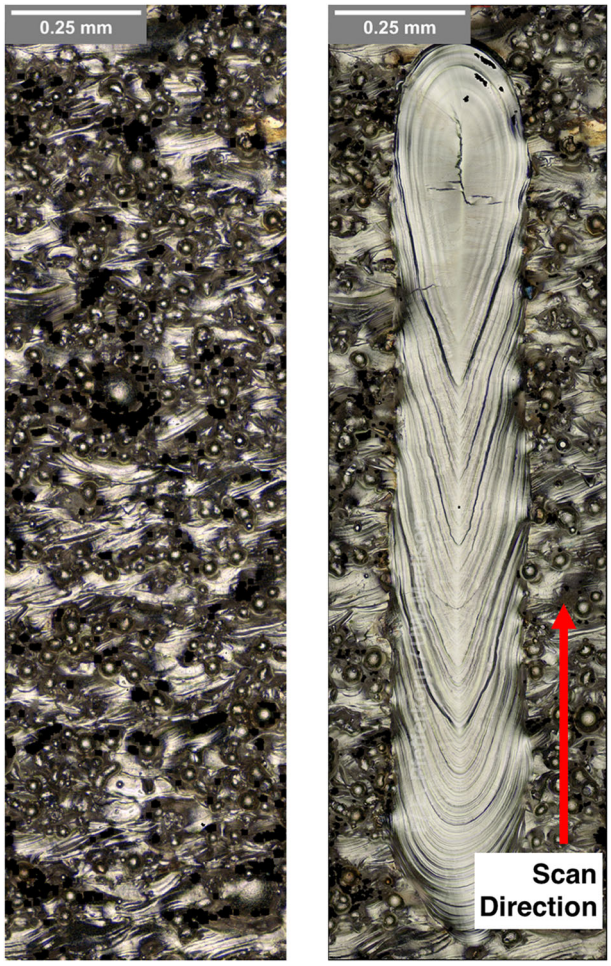

Fig. 2. Surface of the part (a) before and (b) after laser polishing.

$$\text{Energy Density} = \frac{P}{vD} \tag{2}$$

where P, D, and v are the laser power, spot diameter, and velocity, respectively. The experiment used a randomized 2^3 full-factorial experimental design with a center point. The full set of conditions are presented in Table II.

The surface was imaged before and after laser polishing using an optical focus-variation microscope (Alicona InfiniteFocus G4). Reference lines were used to measure the same regions before and after polishing, allowing comparison of the actual polished surface with the predicted laser polished surface. Images of the surface before laser polishing were taken using a 20× objective at vertical and horizontal resolution of 75 nm and 1.25 μm, respectively. Images of the surface after laser polishing were taken using a 50× objective at the same vertical and horizontal resolution of 75 nm and 1.25 μm, respectively. These different objectives were used because the 50× objective could better capture the features in the reflective melt pool. The surface roughness presented is the arithmetical mean height of the surface and was calculated in accordance with ISO 25178.[33] The roughness reductions presented in Table II and Figs. 7 and 8 were calculated as

$$\text{Roughness Reduction } (\%) = \left|\frac{S_{a_{\text{after}}} - S_{a_{\text{before}}}}{S_{a_{\text{before}}}}\right| \times 100\% \tag{3}$$

where $S_{\text{a,before}}$ is the average roughness of the surface before polishing and $S_{\text{a,after}}$ is the average roughness of the surface after laser polishing. Equation 3 was used to calculate the roughness reduction for both the measured and predicted final surface. Only the center 1 mm of the 1.5-mm-long laser-polished lines was used to calculate the roughness, to minimize end effects from the start and stop of the laser.

Melt Duration and Critical Frequency Estimation

The melt duration was estimated by comparing the experimental remelted lines with those given by the solution to the three-dimensional heat equation at the surface of the substrate for steady-state conditions,[34] calculated using the Fourier-transform spectral method.[35] For this alloy at the experimental conditions used, the solidification front was visible within the melt track, which allowed for measurement of what is referred to as the "melt tail." The length of the melt tail was measured on the experimental surface at five different locations, and the mean was used in estimating the total melt length. The mean and standard deviation of the measurements are presented in Table III. The measured melt tail for one condition is shown in Fig. 3a, and an example of a simulated melt tail and total melt length is shown in Fig. 3b. The dark regions seen within the melt track of Fig. 3a are where the microscope could not capture data due to the reflected light being either too bright or too dark. Similar features can be seen in white instead of black in Fig. 6.

Table II. Laser polishing experimental design

	Beam velocity (mm/s)	Beam diameter (μm)	Beam flux (kW/mm^2)	Beam power (W)	Energy density (J/mm^2)
Center pt.	250	125	9.0	111	3.55
C1	200	150	11.3	200	6.67
C2	200	100	11.3	89	4.45
C3	200	100	6.8	53	2.65
C4	300	100	11.3	89	2.97
C5	300	150	6.8	120	2.67
C6	200	150	6.8	120	4.00
C7	300	150	11.3	200	4.44
C8	300	100	6.8	53	1.77

Table III. Measured and estimated melt pool geometry and critical frequency (values given as mean ± standard deviation)

	Measured tail length (μm)	Measured width (μm)	Estimated melt length (μm)	Estimated melt duration (ms)	Residence time (ms)	Predicted critical frequency (mm^{-1})
Center pt.	120 ± 15	136 ± 11	254	1.01	0.50	4.78
C1	366 ± 72	255 ± 13	501	2.50	0.75	3.05
C2	107 ± 11	132 ± 07	196	0.98	0.50	4.87
C3	69 ± 25	93 ± 12	95	0.47	0.50	7.00
C4	119 ± 16	113 ± 04	187	0.62	0.33	6.10
C5	164 ± 26	137 ± 17	272	0.91	0.50	5.06
C6	143 ± 10	164 ± 09	286	1.43	0.75	4.03
C7	280 ± 46	196 ± 17	486	1.62	0.50	3.79
C8	74 ± 19	81 ± 11	86	0.29	0.33	9.00

The simulated tail length ($L_{\text{tail, simulated}}$) was found to follow a linear relationship with both the measured melt tail ($L_{\text{tail, measured}}$) as well as the simulated total length ($L_{\text{total, simulated}}$):

$$(L_{\text{tail, measured}}) \approx C_1 L_{\text{tail, simulated}} + C_2 \quad (4)$$

$$(L_{\text{tail, stimulated}}) \approx C_3 L_{\text{total, simulated}} + C_4 \quad (5)$$

where C_1–C_4 are linear fitting constants. It is assumed that the length of the melt pool is approximately equal to the simulated total melt length multiplied by the aspect ratio between the actual and simulated melt tail length. Using this assumption and Eqs. 4 and 5, a relationship between the simulated total length and the estimated actual length (L_{melt}) can be derived as

$$L_{\text{melt}} \approx \frac{L_{\text{tail, measured}}}{L_{\text{tail, simulated}}} (L_{\text{total, simulated}}) \quad (6)$$

$$L_{\text{melt}} \approx \frac{C_1(C_3 L_{\text{total, simulated}} + C_4) + C_2}{C_3 L_{\text{total, simulated}} + C_4} L_{\text{total, simulated}} \quad (7)$$

Knowing the actual melt length and the beam velocity (v_{beam}), the melt time (t_{melt}) for the center of the melt track can be calculated as

$$t_{\text{melt}} \approx \frac{L_{\text{melt}}}{v_{\text{beam}}} \quad (8)$$

Equations 7 and 8 were used to estimate the melt duration for each of the laser-polishing conditions presented in Table I.

Capillary Smoothing Surface Prediction

Prior work derived a critical frequency above which significant smoothing is expected to occur during pulsed laser polishing due to capillary forces.[22] While the critical frequency concept has previously only been applied to pulsed laser polishing,[22–24,26,36–39] this work tests its suitability for continuous-wave laser polishing. Knowing the melt time through Eq. 8, the critical frequency for these laser polishing experiments can be predicted. The critical frequency was later used to create a surface prediction model that represented the surface smoothing from capillary forces as a low-pass Gaussian filter.[23] Equations 9 and 10 describe the critical frequency and Gaussian filter calculations used for the capillary smoothing surface prediction, respectively:

$$f_{\text{cr}} = \sqrt{\frac{\rho}{8\pi^2 \mu t_{\text{melt}}}} \quad (9)$$

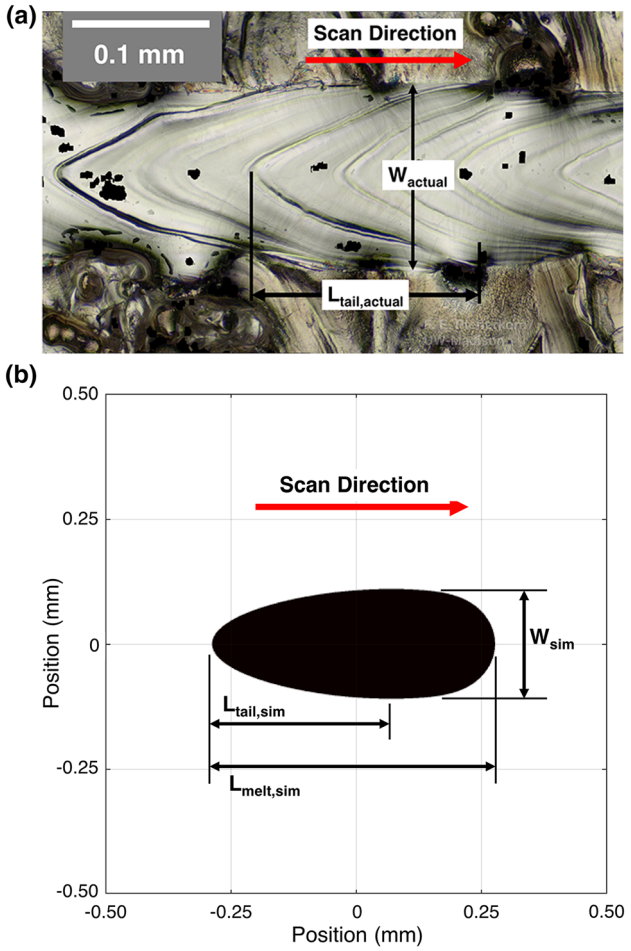

Fig. 3. (a) Measured and (b) simulated melt pool.

$$\zeta(f_x,f_y)_{\text{polished}} = \zeta(f_x,f_y)_{\text{unpolished}} e^{-\left[\left(\frac{f_x}{f_{\text{cr}}}\right)^2+\left(\frac{f_y}{f_{\text{cr}}}\right)^2\right]} \quad (10)$$

where f_{cr} is the critical frequency, ρ and μ are the density and viscosity of the alloy being studied, f_x, and f_y are the frequencies in the x- and y-direction, and ζ is the amplitude of those frequencies. For this work, as the surface imaging was not able to completely capture all roughness features (as seen in Figs. 3a and 6), linear interpolation was used to estimate the regions with missing data. The surfaces with interpolated regions were used for the prediction of the new surface features, but were removed from the predicted surface prior to performing roughness calculations.

RESULTS AND DISCUSSION

Melt Duration and Critical Frequency

The relationships between the measured melt tail length, simulated melt tail length, and simulated melt length are shown in Fig. 4. Figure 4a demonstrates that the simulated melt tail length was a good predictor of the measured tail length. The differences between the simulated and measured

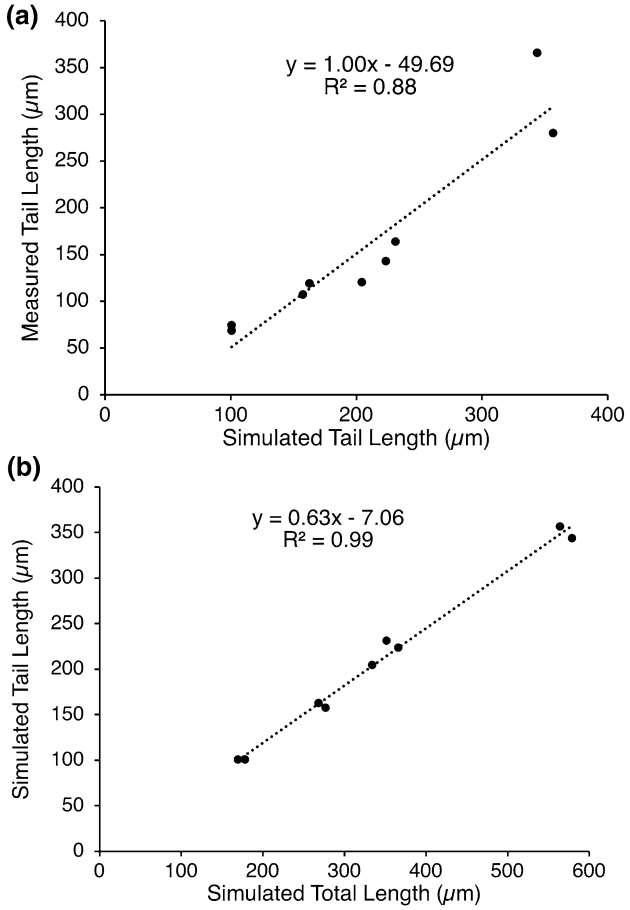

Fig. 4. Relationship between the simulated tail length and (a) the measured tail length and (b) the simulated total length.

values are likely due to the thermal model not including the heat of fusion or thermophysical properties as functions of temperature, and the increase in differences in the melt pool temperature that can occur once convection occurs. Figure 4b shows that the simulated total length and simulated melt tail length were strongly correlated. From these fits, the relationship between the simulated melt length and estimated actual melt length can be predicted as

$$L_{\text{melt}} \approx \frac{1.00(0.63L_{\text{total, simulated}} - 7.06) - 49.69}{0.63L_{\text{total, simulated}} - 7.06} \times L_{\text{total, simulated}} \quad (11)$$

The melt lengths estimated using Eq. 11, and the corresponding melt durations and critical frequencies, are presented in Table III. The residence time is defined as the maximum duration that the beam is over a region and can be calculated by dividing the beam diameter by the beam velocity.

The estimated melt duration ranged from 0.29 ms to 2.50 ms. The residence time, which can be used to give an order estimation of the melt time, ranged from 0.33 ms to 0.75 ms. This demonstrates the unsuitability of using the residence time to

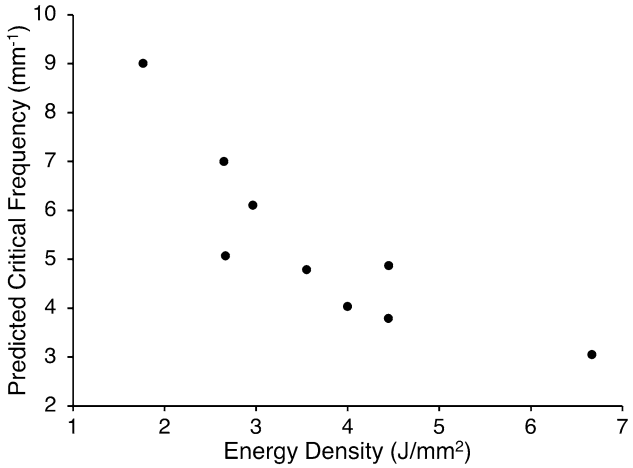

Fig. 5. Relationship between energy density and predicted critical frequency.

approximate the melt duration; however, the residence time does appear to provide an approximate minimum bound on the melt duration. The relationship between the energy density and the predicted critical frequency is shown in Fig. 5. The energy density appears to be a reasonable predictor of the critical frequency, with higher energy densities giving lower critical frequencies. As the critical frequency defines the surface frequencies above which significant smoothing occurs, this implies that higher energy densities would demonstrate better smoothing than lower energy densities. The critical frequency is also inversely related to the melt duration, indicating that higher energy densities cause longer melt times.

Predicted Versus Actual Surface

Figure 6 shows an example of the initial, final, and predicted surfaces for one of the nine laser-polished conditions, and demonstrates that the capillary prediction model captures the general redistribution of the surface features following laser polishing. However, the prediction model redistributes features in the x- and y-directions equally while the actual final surface shows greater redistribution of surface features in the direction of beam travel. This implies that treating the melt time within the center of the melt track is not satisfactory for capturing the physics occurring during continuous-wave laser polishing. The initial, predicted, and actual surface roughness values are presented in Table IV.

The results in Table IV show that a large variation in roughness can occur across different lines. This is also likely to occur within the regions where laser polishing is commonly performed on additively manufactured surfaces. This indicates that work studying the roughness within areas following laser polishing should ensure either that regions with different laser polishing conditions have similar

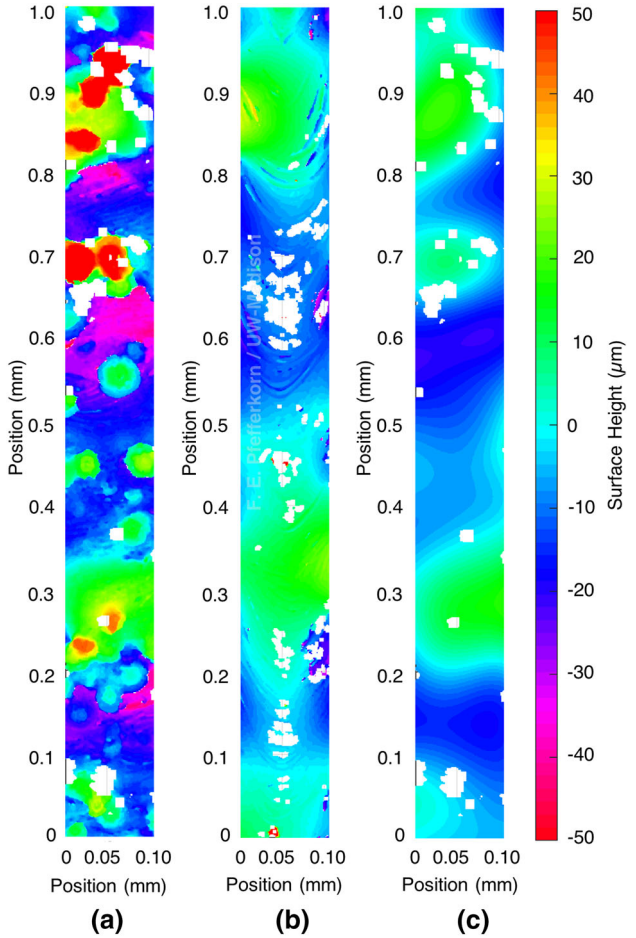

Fig. 6. (a) Initial surface before laser polishing, (b) final surface following laser polishing, and (c) predicted surface for condition C2. All surfaces use the same color scale.

starting roughness, or that enough repetitions are performed to reach a statistically significant sample size. Figure 7 shows the relationship between the critical frequency and the final roughness reduction, while Fig. 8 shows the relationship between the predicted and final roughness reductions.

Figure 7 shows that the predicted critical frequency is inversely related to the final roughness reduction, which would be expected based on Eq. 10. However, there is scatter within the data, which may be due to the inadequacies using the capillary smoothing model with continuous-wave laser polishing. Figure 8 shows that the predicted and final surface roughnesses are approximately proportional to one another, with the prediction slightly underpredicting the final surface roughness. This underprediction may be due to additional flow within the melt pool dispersing roughness features further than predicted by the critical frequency model. One cause for such additional flow may be inertia transmitted into the melt pool from surface tension forces during particle incorporation. Figure 8 also shows scatter in the data, indicating that the capillary smoothing prediction model may under-

Table IV. Roughness values for initial, final, and predicted surface

	Initial surface roughness (S_a) (μm)	Final surface roughness (S_a) (μm)	Predicted surface roughness (S_a) (μm)
Overall surface	20.96	–	–
Center pt.	18.92	6.56	9.16
C1	20.19	6.51	8.69
C2	18.81	7.91	8.25
C3	15.28	11.19	8.90
C4	18.05	7.97	7.27
C5	17.80	12.19	12.65
C6	13.77	6.88	7.83
C7	22.34	6.75	11.15
C8	23.09	11.37	14.60

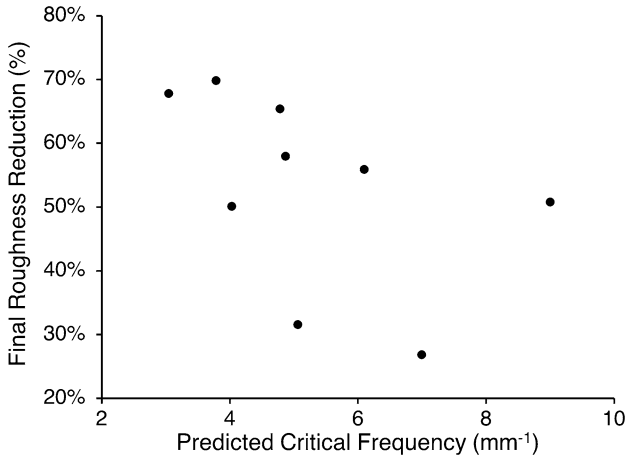

Fig. 7. Final roughness reduction versus predicted critical frequency.

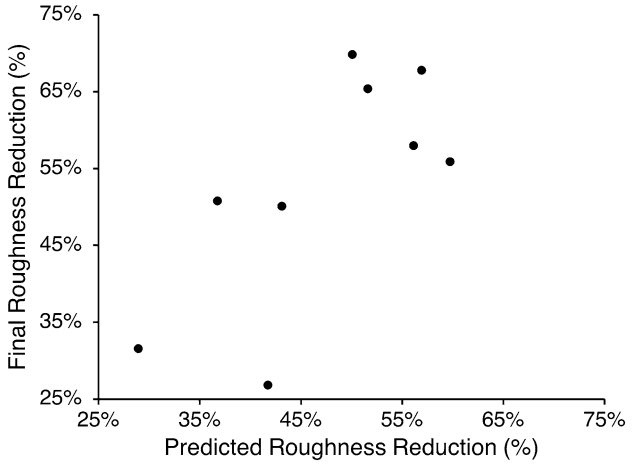

Fig. 8. Final roughness reduction versus predicted roughness reduction.

or overpredict by 15% or more. This also prompts further investigation into a model that could better predict the surface following continuous-wave laser polishing.

CONCLUSION

This work demonstrates the suitability of the critical frequency and capillary smoothing prediction model for continuous-wave laser polishing. To estimate the critical frequency, an estimation for the melt duration had to be derived using measured features in the melt pool and a temperature prediction model. The method presented for melt duration estimation could be applied to a range of metallic alloys, but further work must be done to verify its predictive ability when both interpolating and extrapolating from the laser parameters used. It was observed that the energy density was a reasonable parameter for estimating the melt duration and critical frequency. This work also demonstrates that, while the capillary smoothing prediction model can capture the general smoothing behavior during continuous-wave laser polishing and approximate the final surface roughness, there are several inadequacies that prompt further work on a surface prediction model that could achieve higher accuracy in estimating the surface topography as a result of continuous-wave laser polishing.

ACKNOWLEDGEMENTS

This work was partially supported by U.S. National Science Foundation (NSF) grant CMMI-1727366 and NSF-supported shared facilities at the University of Wisconsin, as well as by the Deutsche Forschungsgemeinschaft (DFG, German Research Foundation, 386371584).

REFERENCES

1. S.A.M. Tofail, E.P. Koumoulos, A. Bandyopadhyay, S. Bose, L. O'Donoghue, and C. Charitidis, *Mater. Today* 21, 22 (2018).
2. K.S. Chan, M. Koike, R.L. Mason, and T. Okabe, *Metall. Mater. Trans. A* 44, 1010 (2013).
3. G. Strano, L. Hao, R.M. Everson, and K.E. Evans, *J. Mater. Process. Technol.* 213, 589 (2013).
4. A. Townsend, N. Senin, L. Blunt, R.K. Leach, and J.S. Taylor, *Precis. Eng.* 46, 34 (2016).
5. A. Thompson, N. Senin, C. Giusca, and R. Leach, *CIRP Ann.* 66, 543 (2017).

6. D.A. Hollander et al., *Biomaterials* 27, 955 (2006).
7. G. Pyka et al., *Adv. Eng. Mater.* 14, 363 (2017).
8. E. Łyczkowska, P. Szymczyk, B. Dybała, and E. Chlebus, *Arch. Civ. Mech. Eng.* 14, 586 (2014).
9. A. Lamikiz, J.A. Sánchez, L. de Lacalle, L. Norberto, D. del Pozo, and J.M. Etayo, *Mater. Sci. Forum* 526, 217 (2006).
10. J.A. Ramos-Grez and D.L. Bourell, *Int. J. Mater. Prod. Technol.* 21, 297 (2004).
11. A. Lamikiz, J.A. Sánchez, L.N. López de Lacalle, and J.L. Arana, *Int. J. Mach. Tools Manuf.* 47, 2040 (2007).
12. J.-P. Kruth, M. Badrossamay, E. Yasa, J. Deckers, L. Thijs, and J. Van Humbeeck, Part and material properties in selective laser melting of metals, in *Proceedings of the 16th International Symposium on Electromachining*, pp. 1–12 (2010).
13. B. Rosa, P. Mognol, and J. Hascoët, *J. Laser Appl.* 27, S29102 (2015).
14. B. Rosa, P. Mognol, and J.-Y. Hascoët, *Rapid Prototyp. J.* 22, 956 (2016).
15. J. Schanz, M. Hofele, L. Hitzler, M. Merkel, and H. Riegel, *Mach. Join Modif. Adv. Mater.* 34, 159 (2016).
16. W.S. Gora et al., *Phys. Procedia* 83, 258 (2016).
17. V. Alfieri, P. Argenio, F. Caiazzo, and V. Sergi, *Materials* 10, 30 (2016).
18. D. Bhaduri et al., *Appl. Surf. Sci.* 405, 29 (2017).
19. J.A. Ramos, J. Murphy, K. Wood, D.L. Bourell, and J.J. Beaman, Surface roughness enhancement of indirect-SLS metal parts by laser surface polishing, in *Solid Freeform Fabrication Proceedings*, pp. 28–38 (2001).
20. J.A. Ramos, D.L. Bourell, and J.J. Beaman, Surface overmelt during laser polishing of indirect-SLS metal parts, in *MRS Proceedings*, vol. 758 (2002).
21. T.M. Shao, M. Hua, H.Y. Tam, and E.H.M. Cheung, *Surf. Coat. Technol.* 197, 77 (2005).
22. T.L. Perry, D. Werschmoeller, N.A. Duffie, X. Li, and F.E. Pfefferkorn, *J. Manuf. Sci. Eng.* 131, 0210021 (2009).
23. M. Vadali, C. Ma, N.A. Duffie, X. Li, and F.E. Pfefferkorn, *J. Manuf. Process.* 14, 307 (2012).
24. C. Ma, M. Vadali, N.A. Duffie, F.E. Pfefferkorn, and X. Li, *J. Manuf. Sci. Eng.* 135, 061023 (2013).
25. C. Ma, M. Vadali, X. Li, N.A. Duffie, and F.E. Pfefferkorn, *J. Micro Nano-Manuf.* 2, 021010 (2014).
26. Q. Wang, J.D. Morrow, C. Ma, N.A. Duffie, and F.E. Pfefferkorn, *J. Manuf. Process.* 20, 340 (2015).
27. P. Johnson and R. Christy, *Phys. Rev. B* 9, 5056 (1974).
28. Stellite 21 Alloy Technical Data, Deloro Stellite, http://exocor.com/downloads/product-datasheets/Stellite-21-Datasheet.pdf.
29. D.G. Farwick and R.N. Johnson, *Thermophysical Properties of Selected Wear-Resistant Alloys* (Richland: Hanford Engineering Development Lab, 1980).
30. Metal Powder and Continuous Casting Rods, Böhler Welding. http://www.bohlerwelding.ru/files/cat/metallpulver.pdf.
31. M.J. Assael, I.J. Armyra, J. Brillo, S.V. Stankus, J. Wu, and W.A. Wakeham, *J. Phys. Chem. Ref. Data* 41, 033101 (2012).
32. E. Ukar, A. Lamikiz, L.N. López de Lacalle, D. del Pozo, and J.L. Arana, *Int. J. Mach. Tools Manuf.* 50, 115 (2010).
33. ISO 25178-1:2016(en), *Geometrical Product Specifications (GPS) Surface Texture: Areal: Part 1: Indication of Surface Texture.*.
34. J.M. Dowden, *The Mathematics of Thermal Modeling: An Introduction to the Theory of Laser Material Processing* (Boca Raton: CRC Press, 2001).
35. G.R.B.E. Römer and A.J. Huisint Veld, *Phys. Procedia* 5, 413 (2010).
36. T.L. Perry, D. Werschmoeller, X. Li, F.E. Pfefferkorn, and N.A. Duffie, *J. Manuf. Sci. Eng.* 131, 031002 (2009).
37. T.L. Perry, D. Werschmoeller, X. Li, F.E. Pfefferkorn, and N.A. Duffie, *J. Manuf. Process.* 11, 74 (2009).
38. F.E. Pfefferkorn, N.A. Duffie, X. Li, M. Vadali, and C. Ma, *CIRP Ann.* 62, 203 (2013).
39. M. Vadali, C. Ma, N.A. Duffie, X. Li, and F.E. Pfefferkorn, *J. Micro Nano Manuf.* 1, 011006 (2013).